

**Supporting information for:**

**Accelerating membrane simulations with**

**Hydrogen Mass Repartitioning**

Curtis Balusek,<sup>†,||</sup> Hyea Hwang,<sup>‡,||</sup> Chun Hon Lau,<sup>¶</sup> Karl Lundquist,<sup>†</sup> Anthony Hazel,<sup>†</sup> Anna Pavlova,<sup>†,⊥</sup> Diane L. Lynch,<sup>§</sup> Patricia H. Reggio,<sup>§</sup> Yi Wang,<sup>\*,¶</sup> and James C. Gumbart<sup>\*,†,⊥</sup>

*†School of Physics, Georgia Institute of Technology, Atlanta, GA 30332*

*‡School of Materials Science and Engineering, Georgia Institute of Technology, Atlanta, GA 30332*

*¶Department of Physics, The Chinese University of Hong Kong, Shatin, N.T., Hong Kong*

*§Department of Chemistry and Biochemistry, University of North Carolina, Greensboro, NC 27402*

*|| Contributed equally to this work*

*⊥School of Chemistry and Biochemistry, Parker H. Petit Institute for Bioengineering and Bioscience, Georgia Institute of Technology, Atlanta, GA 30332*

E-mail: yiwang@cuhk.edu.hk; gumbart@physics.gatech.edu

Table S1: Summary of systems simulated in this work.

System	Lipid Top:Bottom	Atom Count	H <sub>2</sub> O/Lipid	Ions
DPPC	240:240	113064	35.1	84
POPE	240:240	107969	33.3	80
DOPC	240:240	122505	39.0	96
Top6	PMPE 116:116 POPE 32:32 QMPE 32:32 PMPG 24:24 PYPG 20:20 OYPE 16:16	109605	35.3	176
OmpF	POPE 88:88	99154	115.8	819
GPCR	POPC 83:75	89308	124.3	126
L8	POPE 53:52	26696	39.6	0
POPC:CHL	POPC 70:70 CHL 35:35	44012	31.8	38
POPC	340:340	170844	39.0	152

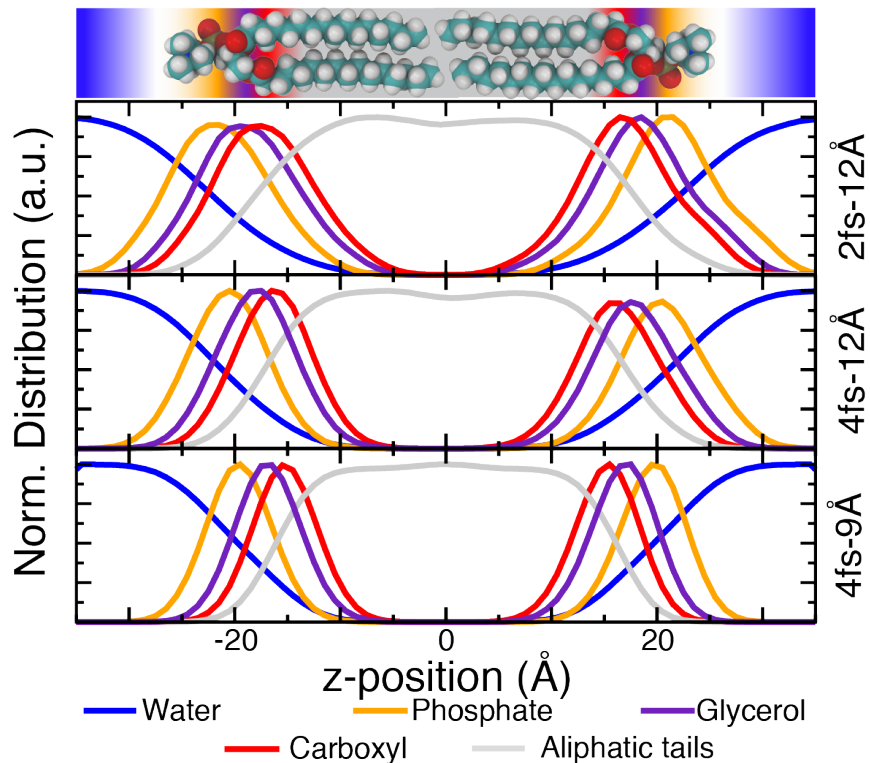


Figure S1: Plot of molecular densities of DPPC in the 2-12 (top), 4-12 (middle), and 4-9 (bottom) simulations. The overlap in aliphatic tails (grey) is shown to increase from 2-12 and 4-12 to 4-9, suggesting that the shorter (9-Å) cutoff compresses and interdigitates the lipid tails more than the 12-Å cutoff.

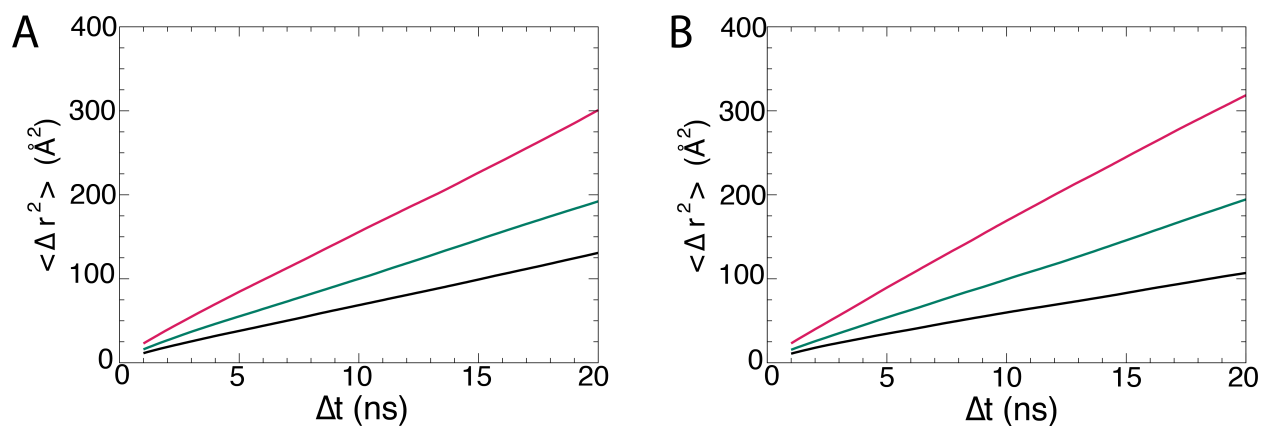


Figure S2: Mean-squared displacement plot of DPPC lipids simulated using (A) Langevin dynamics with a damping constant of  $0.1 \text{ ps}^{-1}$  and (B) the Lowe-Anderson thermostat. The 2-12 simulations are shown in black, 4-12 in green, and 4-9 in red.

Table S2: Diffusion constants (in  $\text{\AA}^2/\text{ns}$ ) measured in 100-ns DPPC membrane simulations at 323 K. Each row is a different thermostat and each column a different protocol. See main text for description of each protocol.

Thermostat	2-12	4-12	4-9	2-12-HMR	2-12-CA	2-9
Langevin ( $\gamma = 1.0 \text{ ps}^{-1}$ )	1.32	1.37	2.27	1.04	1.54	1.96
Langevin ( $\gamma = 0.1 \text{ ps}^{-1}$ )	1.55	2.30	3.59	–	–	–
Lowe-Andersen	1.23	2.33	3.89	–	–	–

Table S3: Temperature as a function of simulation protocol and thermostat used.  $\gamma$  is the damping constant in Langevin dynamics. See also Fig. S3. The target temperature in all cases was 323 K.

Protocol	Langevin ( $\gamma = 0.1 \text{ ps}^{-1}$ )	Langevin ( $\gamma = 1.0 \text{ ps}^{-1}$ )	Lowe-Andersen
2-12	$321.6 \pm 1.0 \text{ K}$	$322.0 \pm 0.9 \text{ K}$	$318.6 \pm 0.9 \text{ K}$
4-12	$327.9 \pm 1.1 \text{ K}$	$325.7 \pm 0.9 \text{ K}$	$323.7 \pm 1.1 \text{ K}$
4-9	$327.9 \pm 1.1 \text{ K}$	$325.7 \pm 0.9 \text{ K}$	$323.8 \pm 1.0 \text{ K}$

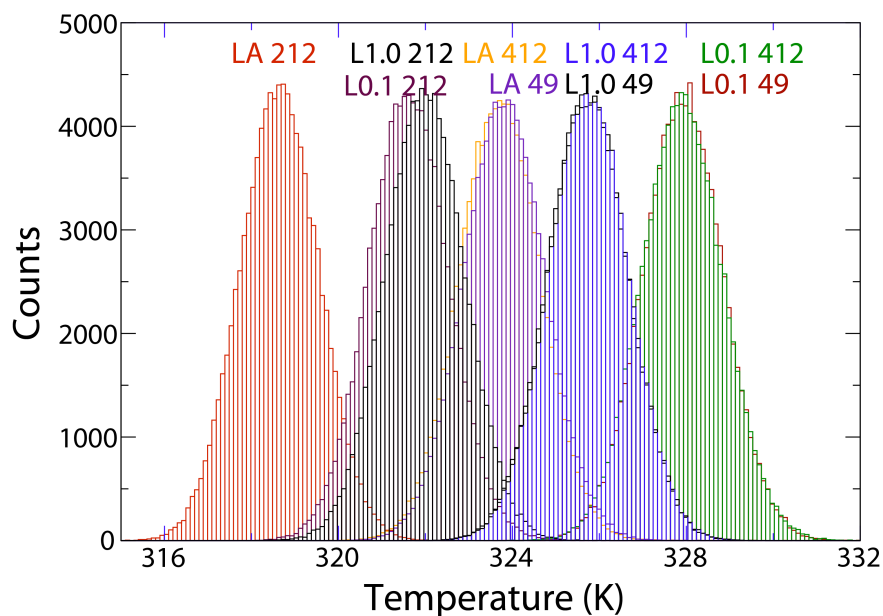


Figure S3: Histograms of the temperatures for each system in Table S3. LA: Lowe-Andersen; L1.0: Langevin dynamics with  $\gamma = 1.0 \text{ ps}^{-1}$ ; L0.1: Langevin dynamics with  $\gamma = 0.1 \text{ ps}^{-1}$ .

Table S4: Dihedral transition rates ( $\text{ns}^{-1}$ ) from Sn1. Black corresponds to the 2-12 DPPC simulation, green to the 4-12, and red to the 4-9.

Dihedral	$G^+ \rightarrow T$	$G^- \rightarrow T$	$T \rightarrow G^+$	$T \rightarrow G^-$	$G^+ \rightarrow G^-$	$G^- \rightarrow G^+$	No $G^+$	No $G^-$	No T
C2-C3-C4-C5	72.51±8.2	69.76±7.88	72.66±8.07	69.42±7.84	12.69±3.69	12.47±3.57	72.55±17.18	69.31±18.95	548.62±39.97
	75.09±7.96	71.92±7.53	75.04±8.13	71.86±7.42	12.67±3.49	12.69±3.68	72.87±16.66	71.89±17.99	535.97±34.79
	81.52±8.19	78.14±8.44	81.26±7.8	78.22±8.45	14.18±3.87	14.38±3.81	72.06±14.63	71.15±16.87	509.08±33.37
C3-C4-C5-C6	98.81±8.98	102.7±8.79	99.12±8.61	102.43±8.89	27.47±5.27	27.19±5.15	55.12±10.94	58.08±10.11	429.07±27.89
	100.52±8.38	102.73±8.5	100.44±8.61	102.8±8.48	26.35±5.02	26.46±4.94	58.0±10.11	60.24±10.36	422.48±26.2
	104.22±8.98	105.88±8.72	104.39±8.81	105.7±8.71	27.81±4.96	27.65±5.43	57.02±10.54	57.34±10.31	409.99±24.92
C4-C5-C6-C7	80.34±8.26	80.46±7.95	80.17±8.22	80.47±7.94	12.75±3.64	12.85±3.54	32.34±8.16	33.12±8.31	587.51±28.73
	82.84±8.31	82.56±8.09	82.45±7.89	82.81±8.29	12.83±3.49	13.16±3.57	34.21±7.36	35.44±8.87	573.7±26.36
	86.88±7.95	87.61±8.07	86.59±8.28	87.73±7.93	13.5±3.6	13.74±3.63	33.45±8.01	34.94±7.84	555.55±25.15
C5-C6-C7-C8	92.98±8.54	93.65±8.45	92.87±8.61	93.66±8.61	17.69±4.19	17.75±4.12	34.88±7.79	34.85±7.52	521.67±25.49
	94.54±8.71	94.67±8.67	94.48±8.32	94.67±8.44	18.01±4.03	18.05±4.08	37.88±7.85	37.28±8.3	510.42±24.57
	98.75±8.67	97.05±8.04	98.64±8.63	97.12±8.25	18.84±4.09	18.95±4.37	37.08±7.95	36.42±7.41	497.15±23.53
C6-C7-C8-C9	82.19±8.66	82.62±8.09	82.41±8.62	82.3±7.94	13.23±3.84	12.97±3.66	27.38±6.92	28.31±7.21	588.58±29.14
	84.85±8.39	85.65±8.14	84.7±8.27	85.69±7.91	13.46±3.48	13.57±3.68	30.32±7.48	30.88±8.02	570.88±27.79
	90.17±8.8	89.39±8.18	90.16±8.4	89.32±8.3	14.58±3.65	14.58±3.72	31.11±7.05	30.95±7.06	549.75±24.31
C7-C8-C9-C10	92.23±8.14	92.08±8.32	92.06±8.28	92.1±8.29	16.6±4.06	16.66±3.97	30.33±6.84	30.65±7.37	537.3±25.04
	94.39±8.54	94.36±8.48	94.05±8.38	94.6±8.2	16.65±4.04	16.93±3.83	33.2±7.32	33.49±7.59	522.33±23.97
	97.5±8.59	97.9±7.91	97.22±8.42	98.14±8.01	17.76±4.03	18.01±4.17	33.22±7.31	32.81±6.93	507.43±21.59
C8-C9-C10-C11	86.28±8.52	86.89±8.59	86.17±8.18	86.86±8.58	14.18±3.61	14.22±3.92	26.57±6.74	27.01±7.06	571.8±28.44
	89.43±8.29	89.82±8.11	89.45±8.11	89.72±8.28	14.85±3.82	14.79±3.86	29.26±7.67	29.57±6.99	553.12±26.15
	93.87±7.96	94.38±8.02	93.87±7.93	94.3±8.0	16.38±3.93	16.36±4.22	29.71±6.91	29.78±7.25	531.39±24.09
C9-C10-C11-C12	96.55±8.79	96.8±8.69	96.61±8.11	96.71±8.53	17.92±4.11	17.85±3.99	31.38±7.34	31.94±7.6	514.95±23.24
	100.37±8.18	100.21±8.61	100.54±8.04	99.99±8.46	19.12±4.52	18.94±4.07	31.94±6.87	31.62±6.98	497.26±22.44
	92.41±8.64	92.84±8.8	92.48±8.53	92.69±8.61	16.74±4.14	16.66±4.0	25.94±5.94	26.36±6.63	543.9±26.21
C10-C11-C12-C13	95.2±8.77	96.14±8.2	95.03±8.87	96.22±8.4	17.42±4.19	17.58±4.36	28.96±6.52	29.01±6.65	524.44±22.56
	99.36±8.27	99.06±8.55	99.73±8.11	98.62±8.14	18.98±3.98	18.6±3.77	29.03±6.34	29.62±6.71	506.99±23.72
	99.58±9.05	99.82±8.5	99.59±8.85	99.74±8.37	19.89±4.23	19.86±4.22	27.1±6.03	27.21±6.15	507.22±23.04
C11-C12-C13-C14	101.09±8.48	101.18±8.26	100.86±8.28	101.31±7.95	20.33±4.39	20.55±4.24	28.92±6.47	29.3±6.66	496.46±24.04
	104.19±8.41	103.53±8.24	104.21±8.24	103.44±8.62	21.35±4.45	21.3±4.58	28.91±6.59	29.01±6.65	484.07±22.34
	101.21±8.25	100.7±8.59	100.85±8.2	100.99±8.49	20.52±4.51	20.86±4.58	25.2±6.02	25.25±5.7	504.42±24.04
C12-C13-C14-C15	102.84±8.78	102.82±8.93	102.63±8.12	102.98±8.62	21.51±4.4	21.71±4.47	27.36±5.72	27.29±6.42	490.87±23.42
	104.34±8.58	105.4±8.54	104.66±8.48	105.02±8.59	22.95±4.57	22.62±4.82	27.12±5.99	27.34±6.41	480.54±22.79
	104.93±8.01	104.98±8.15	105.02±7.94	104.86±8.2	23.1±4.44	23.01±4.8	24.44±5.24	24.48±5.62	485.18±21.71
C13-C14-C15-C16	105.97±8.93	106.05±8.53	106.06±8.85	105.95±8.79	23.74±4.68	23.65±4.33	26.28±5.6	25.77±5.87	476.53±21.71
	106.43±8.51	107.34±8.67	106.79±8.54	106.94±8.87	24.37±4.99	24.02±4.94	25.83±5.75	25.9±5.54	472.38±21.02

Table S5: Dihedral transition rates ( $\text{ns}^{-1}$ ) from Sn2. Black corresponds to the 2-12 DPPC simulation, green to the 4-12, and red to the 4-9.

Dihedral	$G^+ \rightarrow T$	$G^- \rightarrow T$	$T \rightarrow G^+$	$T \rightarrow G^-$	$G^+ \rightarrow G^-$	$G^- \rightarrow G^+$	No $G^+$	No $G^-$	No T
C2-C3-C4-C5	92.7 $\pm$ 8.52	57.92 $\pm$ 7.9	92.99 $\pm$ 8.3	57.68 $\pm$ 7.59	25.74 $\pm$ 4.85	25.49 $\pm$ 4.96	247.5 $\pm$ 36.25	118.87 $\pm$ 23.35	281.16 $\pm$ 37.0
	94.75 $\pm$ 8.68	59.96 $\pm$ 7.39	95.06 $\pm$ 8.06	59.65 $\pm$ 7.25	24.44 $\pm$ 4.67	24.14 $\pm$ 4.65	242.48 $\pm$ 32.1	116.84 $\pm$ 23.31	282.69 $\pm$ 35.76
	102.2 $\pm$ 8.64	63.36 $\pm$ 7.65	102.27 $\pm$ 8.36	63.3 $\pm$ 7.42	25.34 $\pm$ 4.96	25.3 $\pm$ 4.88	228.44 $\pm$ 29.47	107.59 $\pm$ 21.59	282.2 $\pm$ 31.18
C3-C4-C5-C6	80.28 $\pm$ 8.09	88.56 $\pm$ 8.61	80.05 $\pm$ 8.18	88.69 $\pm$ 8.76	14.05 $\pm$ 3.79	14.25 $\pm$ 3.74	42.51 $\pm$ 10.4	42.8 $\pm$ 10.07	548.82 $\pm$ 28.76
	81.42 $\pm$ 7.86	91.14 $\pm$ 8.2	81.59 $\pm$ 7.97	90.82 $\pm$ 8.49	14.37 $\pm$ 3.79	14.16 $\pm$ 3.76	44.33 $\pm$ 10.91	46.05 $\pm$ 9.85	536.12 $\pm$ 28.7
	86.41 $\pm$ 8.19	95.21 $\pm$ 8.28	86.31 $\pm$ 7.98	95.22 $\pm$ 8.34	15.76 $\pm$ 3.84	15.83 $\pm$ 3.75	44.02 $\pm$ 9.98	44.2 $\pm$ 9.42	517.04 $\pm$ 24.95
C4-C5-C6-C7	94.17 $\pm$ 8.42	87.56 $\pm$ 8.49	93.66 $\pm$ 8.27	87.94 $\pm$ 8.28	16.31 $\pm$ 4.14	16.76 $\pm$ 4.1	43.26 $\pm$ 9.4	42.26 $\pm$ 8.81	518.07 $\pm$ 25.51
	95.42 $\pm$ 8.65	88.83 $\pm$ 8.42	95.5 $\pm$ 8.65	88.69 $\pm$ 8.48	16.09 $\pm$ 3.74	15.99 $\pm$ 3.96	45.23 $\pm$ 9.43	44.83 $\pm$ 9.63	509.42 $\pm$ 24.11
	98.02 $\pm$ 8.18	92.49 $\pm$ 8.39	98.13 $\pm$ 8.17	92.3 $\pm$ 8.17	16.62 $\pm$ 4.0	16.46 $\pm$ 3.99	43.43 $\pm$ 8.78	43.03 $\pm$ 9.01	499.53 $\pm$ 23.23
C5-C6-C7-C8	81.31 $\pm$ 7.96	82.7 $\pm$ 7.88	81.12 $\pm$ 8.15	82.81 $\pm$ 8.13	12.74 $\pm$ 3.51	12.86 $\pm$ 3.72	28.65 $\pm$ 7.41	28.61 $\pm$ 7.18	589.2 $\pm$ 26.66
	83.71 $\pm$ 8.36	84.5 $\pm$ 8.55	83.66 $\pm$ 8.4	84.49 $\pm$ 8.82	12.95 $\pm$ 3.37	12.96 $\pm$ 3.49	32.63 $\pm$ 8.05	30.89 $\pm$ 7.64	574.2 $\pm$ 25.28
	87.72 $\pm$ 8.18	89.97 $\pm$ 8.13	87.67 $\pm$ 8.14	89.94 $\pm$ 8.29	14.24 $\pm$ 3.73	14.22 $\pm$ 3.62	31.94 $\pm$ 7.52	31.13 $\pm$ 7.47	553.16 $\pm$ 23.83
C6-C7-C8-C9	88.85 $\pm$ 8.23	88.96 $\pm$ 8.37	89.17 $\pm$ 8.2	88.48 $\pm$ 8.5	15.6 $\pm$ 3.98	15.23 $\pm$ 4.02	31.24 $\pm$ 7.21	31.97 $\pm$ 7.79	550.49 $\pm$ 25.51
	91.41 $\pm$ 8.61	91.08 $\pm$ 8.31	91.34 $\pm$ 8.87	91.06 $\pm$ 8.58	15.75 $\pm$ 4.0	15.83 $\pm$ 3.84	33.57 $\pm$ 7.95	34.55 $\pm$ 7.5	535.41 $\pm$ 24.39
	94.44 $\pm$ 8.36	94.38 $\pm$ 8.79	94.32 $\pm$ 8.45	94.38 $\pm$ 8.09	16.42 $\pm$ 4.06	16.48 $\pm$ 3.99	32.95 $\pm$ 7.28	34.35 $\pm$ 7.56	522.28 $\pm$ 23.38
C7-C8-C9-C10	83.85 $\pm$ 8.21	84.25 $\pm$ 8.13	83.89 $\pm$ 8.04	84.15 $\pm$ 8.59	13.6 $\pm$ 3.7	13.56 $\pm$ 3.57	26.13 $\pm$ 6.77	27.04 $\pm$ 7.06	583.54 $\pm$ 26.83
	86.67 $\pm$ 8.64	86.92 $\pm$ 8.22	87.15 $\pm$ 8.63	86.42 $\pm$ 8.05	14.02 $\pm$ 3.74	13.56 $\pm$ 3.64	29.16 $\pm$ 7.32	28.85 $\pm$ 6.86	567.27 $\pm$ 25.53
	90.83 $\pm$ 7.73	91.86 $\pm$ 7.8	90.94 $\pm$ 7.88	91.71 $\pm$ 8.22	14.85 $\pm$ 3.79	14.74 $\pm$ 3.88	30.14 $\pm$ 6.74	30.0 $\pm$ 6.99	544.94 $\pm$ 24.21
C8-C9-C10-C11	90.47 $\pm$ 8.56	90.24 $\pm$ 8.55	90.36 $\pm$ 8.29	90.27 $\pm$ 8.46	15.94 $\pm$ 3.93	16.04 $\pm$ 4.0	28.11 $\pm$ 7.03	28.9 $\pm$ 7.37	549.66 $\pm$ 25.61
	93.0 $\pm$ 8.19	92.33 $\pm$ 8.33	93.09 $\pm$ 8.66	92.13 $\pm$ 8.53	16.41 $\pm$ 3.76	16.32 $\pm$ 3.73	31.31 $\pm$ 7.45	31.43 $\pm$ 7.12	533.97 $\pm$ 23.19
	96.95 $\pm$ 8.29	96.03 $\pm$ 8.66	96.73 $\pm$ 8.36	96.22 $\pm$ 8.85	17.07 $\pm$ 3.98	17.29 $\pm$ 4.09	31.32 $\pm$ 6.83	31.27 $\pm$ 6.93	517.11 $\pm$ 22.59
C9-C10-C11-C12	88.14 $\pm$ 7.77	88.18 $\pm$ 7.83	88.08 $\pm$ 8.13	88.11 $\pm$ 8.15	14.77 $\pm$ 3.92	14.76 $\pm$ 4.01	25.31 $\pm$ 6.7	25.54 $\pm$ 6.72	567.12 $\pm$ 27.72
	90.51 $\pm$ 8.39	91.74 $\pm$ 8.17	90.6 $\pm$ 8.33	91.6 $\pm$ 8.19	15.52 $\pm$ 3.89	15.43 $\pm$ 3.78	28.23 $\pm$ 6.89	27.9 $\pm$ 6.66	548.48 $\pm$ 24.44
	94.96 $\pm$ 8.79	95.49 $\pm$ 8.31	94.88 $\pm$ 8.74	95.52 $\pm$ 8.42	16.94 $\pm$ 3.95	16.99 $\pm$ 3.94	29.19 $\pm$ 6.9	29.1 $\pm$ 6.55	526.93 $\pm$ 23.16
C10-C11-C12-C13	93.82 $\pm$ 8.1	94.67 $\pm$ 8.72	93.94 $\pm$ 8.34	94.46 $\pm$ 8.73	17.49 $\pm$ 4.13	17.31 $\pm$ 4.14	26.68 $\pm$ 6.48	27.17 $\pm$ 6.73	534.45 $\pm$ 26.2
	96.08 $\pm$ 8.48	96.86 $\pm$ 8.18	96.16 $\pm$ 8.23	96.72 $\pm$ 7.95	17.94 $\pm$ 4.18	17.79 $\pm$ 4.18	29.11 $\pm$ 6.74	29.59 $\pm$ 6.62	519.74 $\pm$ 22.74
	99.58 $\pm$ 9.17	100.05 $\pm$ 8.61	99.73 $\pm$ 8.81	99.88 $\pm$ 8.7	19.08 $\pm$ 4.3	18.91 $\pm$ 4.17	29.39 $\pm$ 6.79	29.39 $\pm$ 6.41	503.99 $\pm$ 23.78
C11-C12-C13-C14	93.73 $\pm$ 8.45	94.62 $\pm$ 8.15	93.77 $\pm$ 8.69	94.52 $\pm$ 8.01	17.5 $\pm$ 3.97	17.46 $\pm$ 3.98	23.75 $\pm$ 5.86	24.76 $\pm$ 6.14	539.89 $\pm$ 24.66
	97.11 $\pm$ 8.73	97.14 $\pm$ 8.49	97.1 $\pm$ 8.48	97.12 $\pm$ 8.41	18.08 $\pm$ 4.31	18.08 $\pm$ 4.36	26.36 $\pm$ 6.29	26.09 $\pm$ 6.34	522.92 $\pm$ 23.06
	100.67 $\pm$ 8.57	100.92 $\pm$ 8.64	100.82 $\pm$ 8.38	100.77 $\pm$ 8.63	20.08 $\pm$ 4.39	19.89 $\pm$ 4.2	26.99 $\pm$ 6.06	27.92 $\pm$ 6.28	502.01 $\pm$ 20.88
C12-C13-C14-C15	101.23 $\pm$ 7.97	99.96 $\pm$ 8.59	100.73 $\pm$ 8.04	100.44 $\pm$ 8.48	20.4 $\pm$ 4.4	20.89 $\pm$ 4.61	24.94 $\pm$ 6.05	25.16 $\pm$ 5.89	506.25 $\pm$ 24.39
	102.54 $\pm$ 8.38	103.05 $\pm$ 8.21	102.64 $\pm$ 8.66	102.9 $\pm$ 8.36	21.45 $\pm$ 4.33	21.36 $\pm$ 4.58	26.99 $\pm$ 6.02	27.36 $\pm$ 5.86	491.71 $\pm$ 21.76
	104.77 $\pm$ 8.34	105.25 $\pm$ 8.4	104.69 $\pm$ 8.68	105.33 $\pm$ 8.97	22.55 $\pm$ 4.44	22.63 $\pm$ 4.58	27.39 $\pm$ 5.99	26.78 $\pm$ 6.14	480.61 $\pm$ 21.48
C13-C14-C15-C16	102.45 $\pm$ 8.58	102.4 $\pm$ 8.67	102.24 $\pm$ 8.4	102.52 $\pm$ 8.36	21.4 $\pm$ 4.54	21.56 $\pm$ 4.41	22.96 $\pm$ 5.32	22.89 $\pm$ 5.41	501.58 $\pm$ 23.36
	104.24 $\pm$ 8.35	104.41 $\pm$ 8.03	104.08 $\pm$ 8.32	104.54 $\pm$ 8.42	22.05 $\pm$ 4.69	22.22 $\pm$ 4.39	24.6 $\pm$ 5.49	24.68 $\pm$ 5.54	489.19 $\pm$ 21.64
	105.32 $\pm$ 8.33	105.78 $\pm$ 8.9	105.28 $\pm$ 8.39	105.71 $\pm$ 8.66	23.04 $\pm$ 4.73	23.04 $\pm$ 4.5	25.09 $\pm$ 5.72	25.38 $\pm$ 5.91	481.35 $\pm$ 21.71

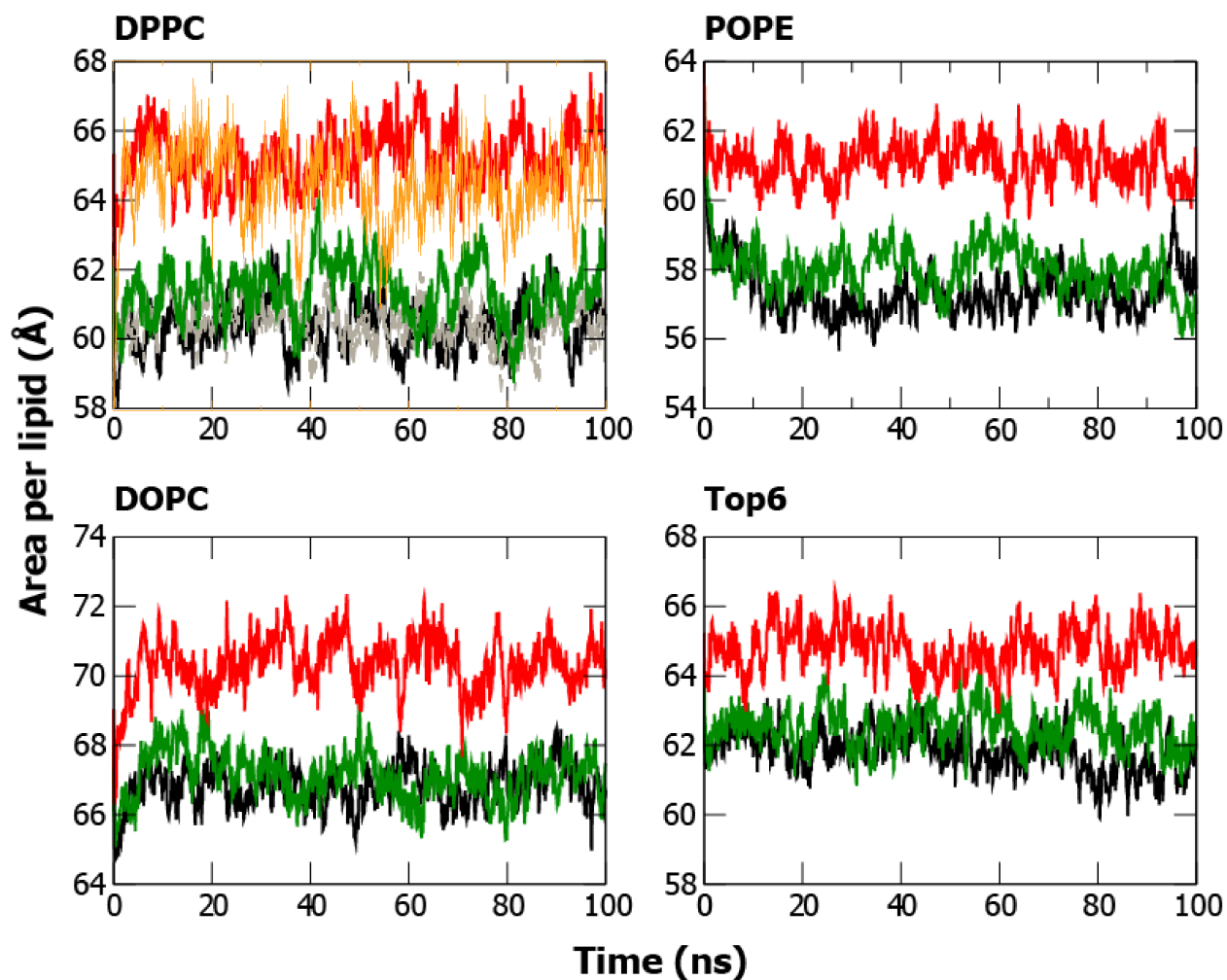


Figure S4: Plots of APL over 100 ns. The averages in Table 1 in the main text were obtained from the last 50 ns of each simulation. In each panel, 2-12 is shown in black, 4-12 in green, and 4-9 in red. A separate 2-12-HMR simulation performed for the DPPC bilayer is shown in grey and one performed with 2-9 parameters is shown in orange (top left).

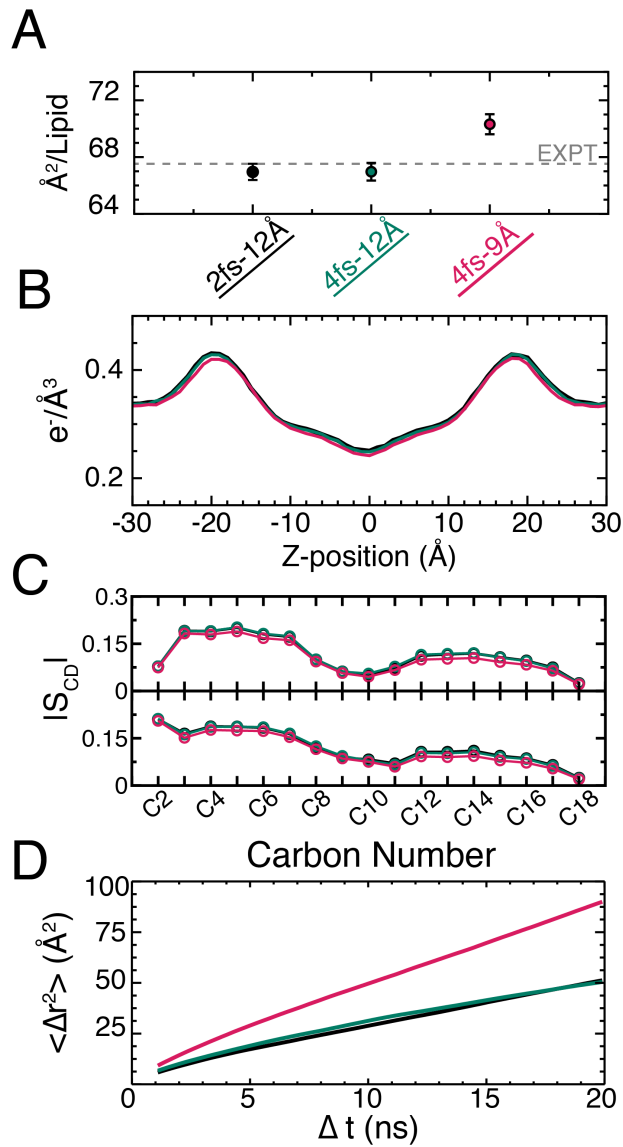


Figure S5: Properties of the DOPC membrane. In all panels, black is the 2-12 protocol, green is the 4-12 protocol, and red is the 4-9 protocol. (A) Area per lipid. (B) Electron Density. (C) Order parameters for Sn2 (top) and Sn1 (bottom). (D) Mean-squared displacement.

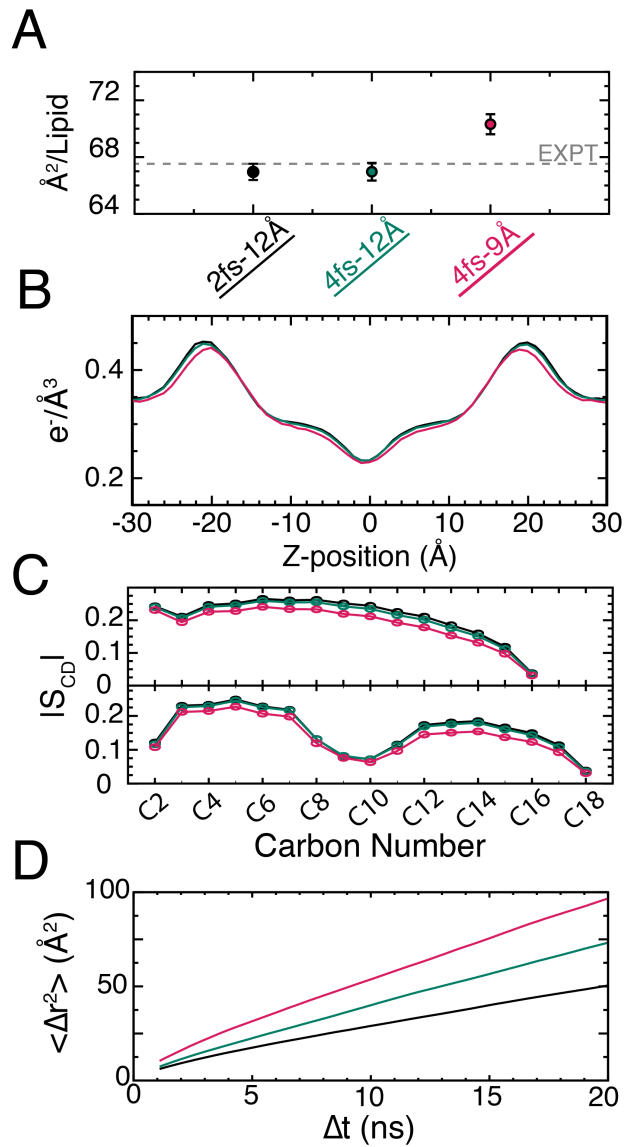


Figure S6: Properties of the POPE membrane. In all panels, black is the 2-12 protocol, green is the 4-12 protocol, and red is the 4-9 protocol. (A) Area per lipid. (B) Electron Density. (C) Order parameters for Sn2 (top) and Sn1 (bottom). (D) Mean-squared displacement.

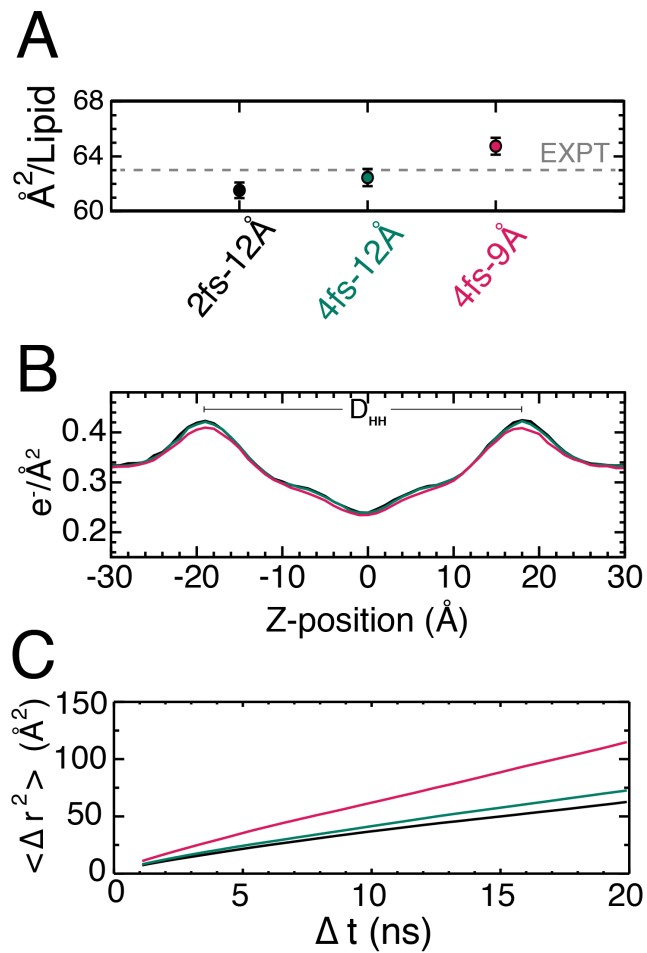


Figure S7: Properties of the Top6 membrane. In all panels, black is the 2-12 protocol, green is the 4-12 protocol, and red is the 4-9 protocol. (A) Area per lipid. (B) Electron Density. (C) Mean-squared displacement.

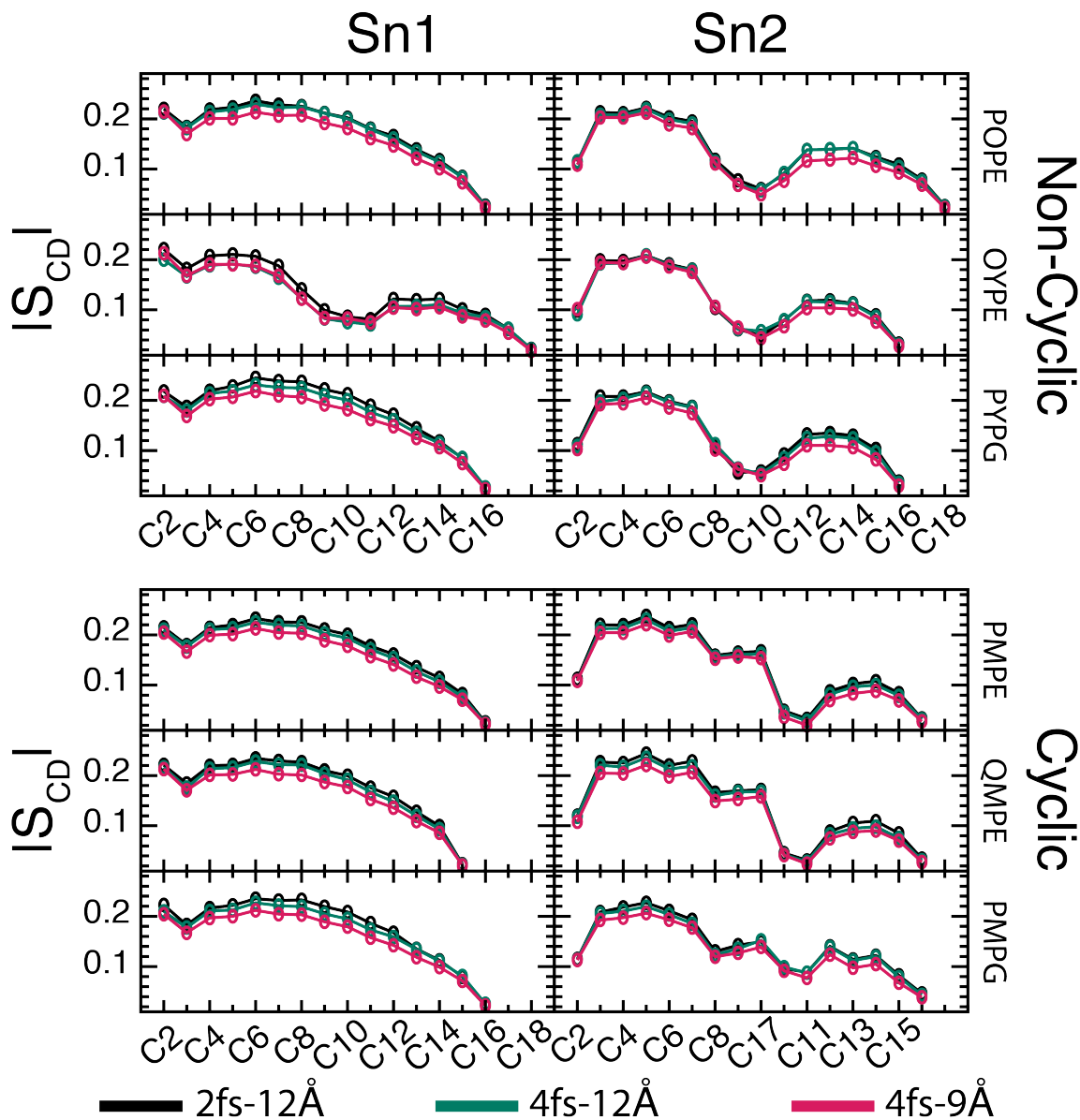


Figure S8: Order parameters for the Top6 membrane. In all panels, black is the 2-12 protocol, green is the 4-12 protocol, and red is the 4-9 protocol. Plots in the left column are the Sn1 tails and those in the right column are Sn2. The upper cluster are non-cyclic tails and the lower group are cyclic-group-containing tails. The bottom right panel has C17 (the cyclic carbon) inserted between C9 and C10.

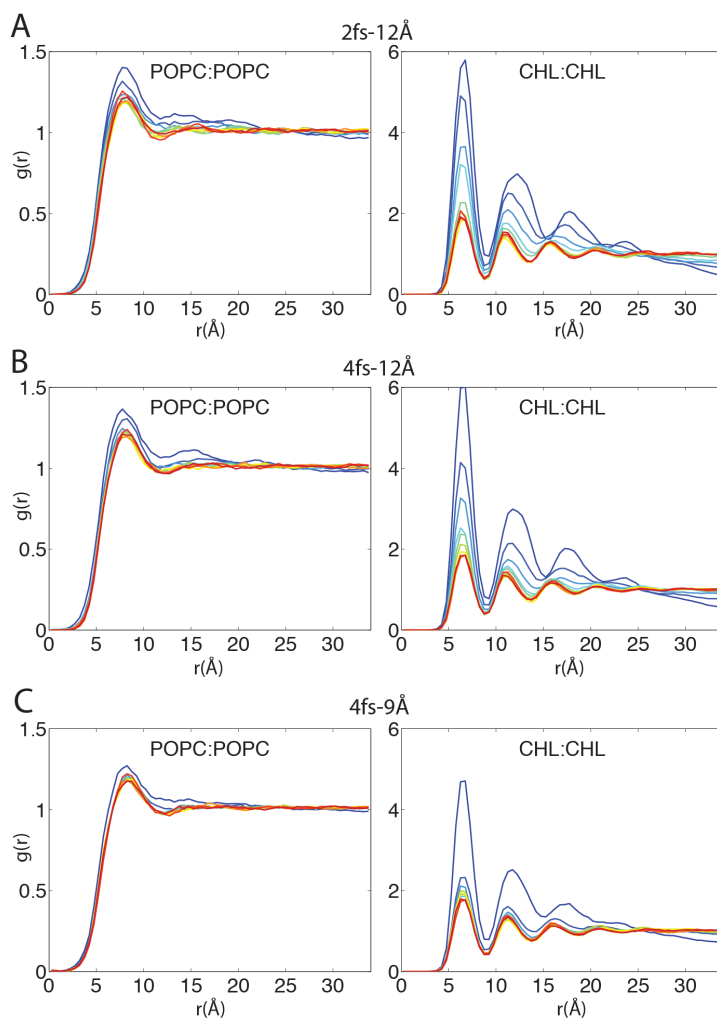


Figure S9: Time evolution of the radial pair distribution functions  $g(r)$  for POPC:POPC and CHL:CHL from the 2-12 (A), the 4-12 (B), and the 4-9 (C) lipid mixing simulations. Calculated  $g(r)$  is averaged in 100-ns blocks and colored by simulation time, with blue, green and red indicating the beginning, the middle and the end of a simulation, respectively.

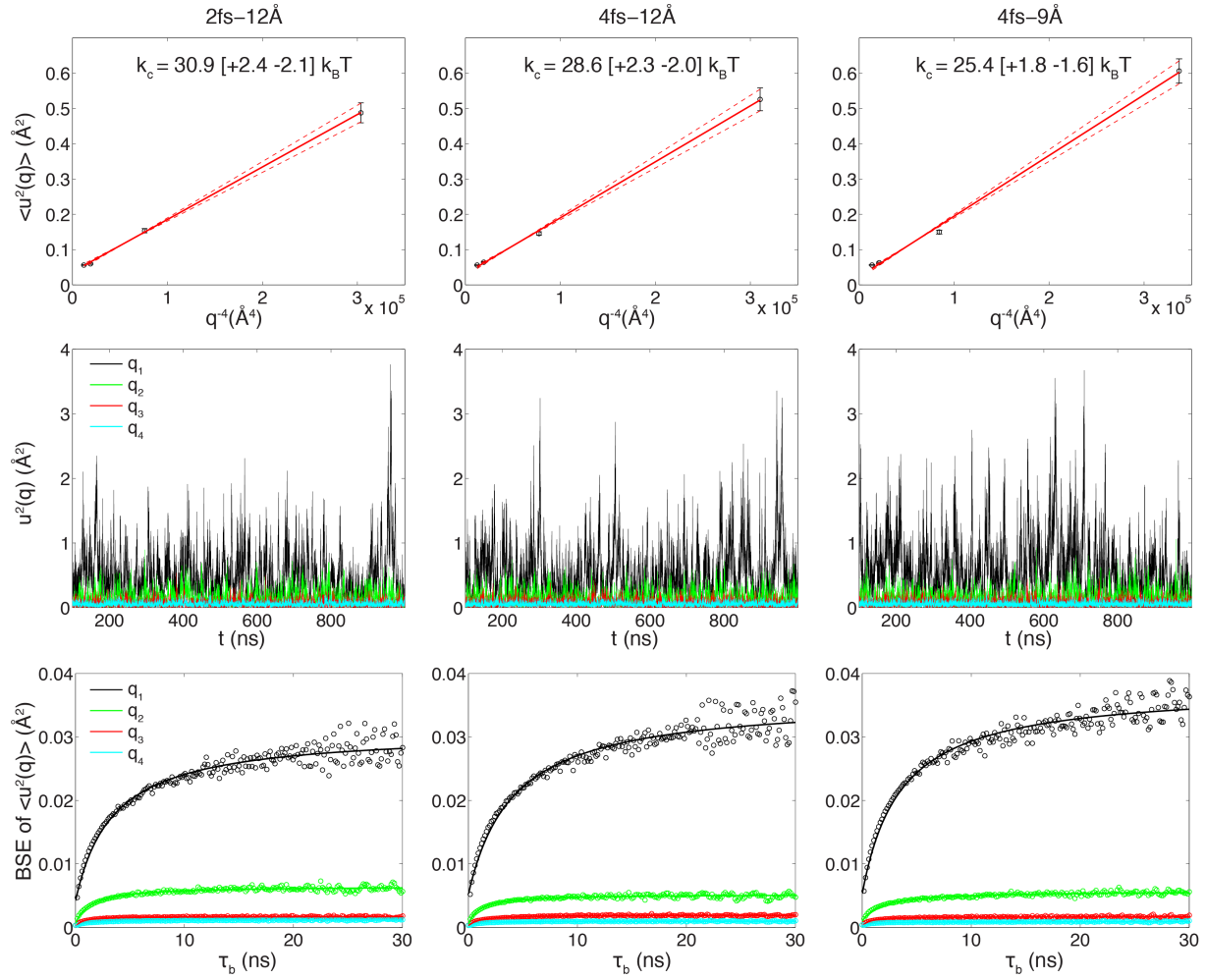


Figure S10: Undulation analysis of a POPC bilayer with 680 lipids. (a) The bending modulus  $k_c$  obtained from the slope of  $\langle u^2(q) \rangle$  versus  $q^{-4}$ . The estimated uncertainty in  $k_c$  is given in square brackets (see Methods for details). (b)  $u^2(q)$  as a function of simulation time. (c) The blocked standard error (BSE) in  $\langle u^2(q) \rangle$  as a function of the block size  $\tau_b$ . Results of the lowest wavenumber ( $q_1 \approx 0.04 \text{ \AA}^{-1}$ ) are colored in black circles, with the black solid curve representing a least square fit using a rational polynomial function. Similarly, results for the next three wavenumbers are colored in green, red and blue, respectively.

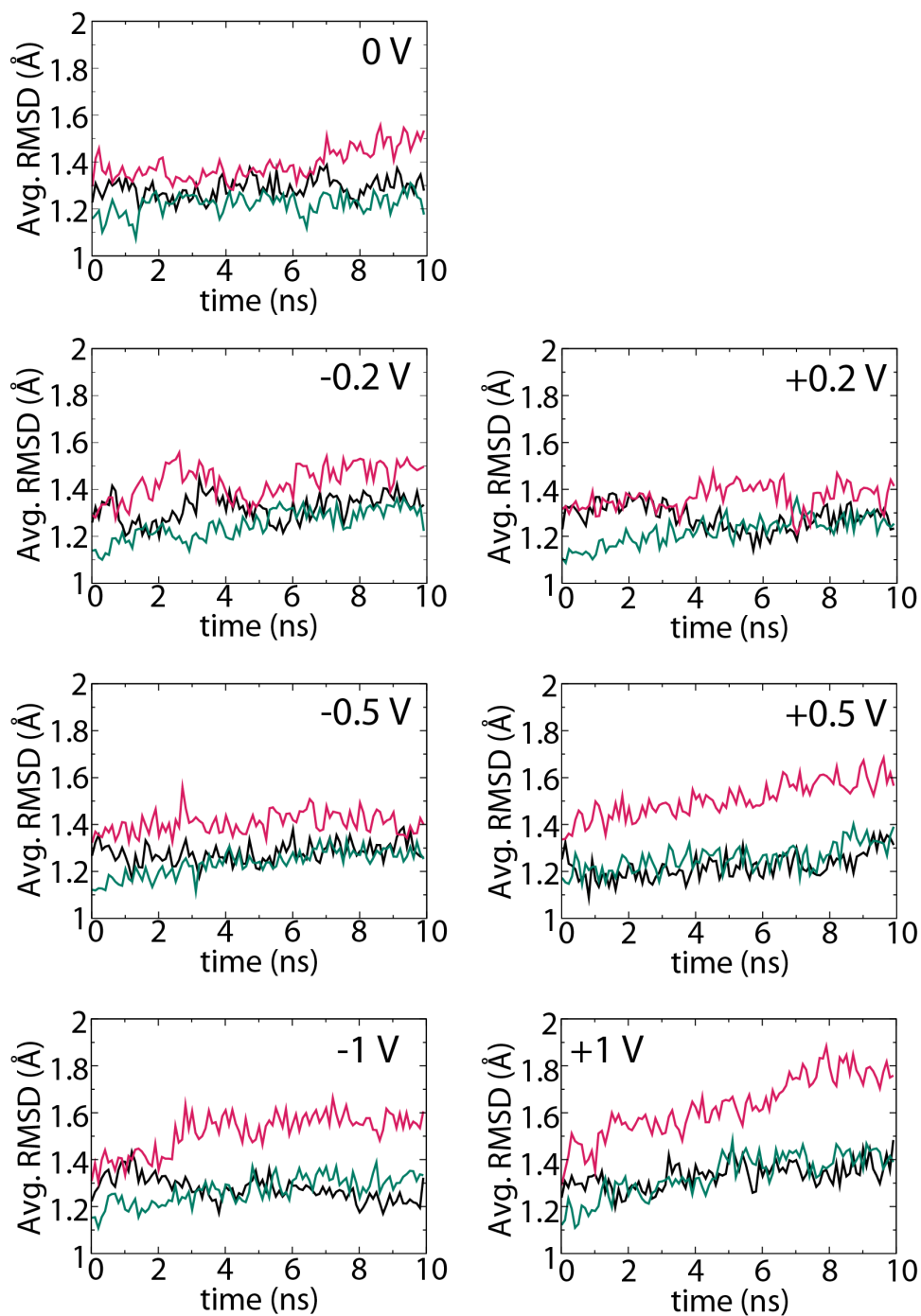


Figure S11: Root mean-square deviation (RMSD) for OmpF trimers in applied electric field simulations. Each line is an average of three independent replicas. The voltage used is indicated in each of the seven graphs. The 2-12 simulations are in black, the 4-12 in green, and the 4-9 in red.

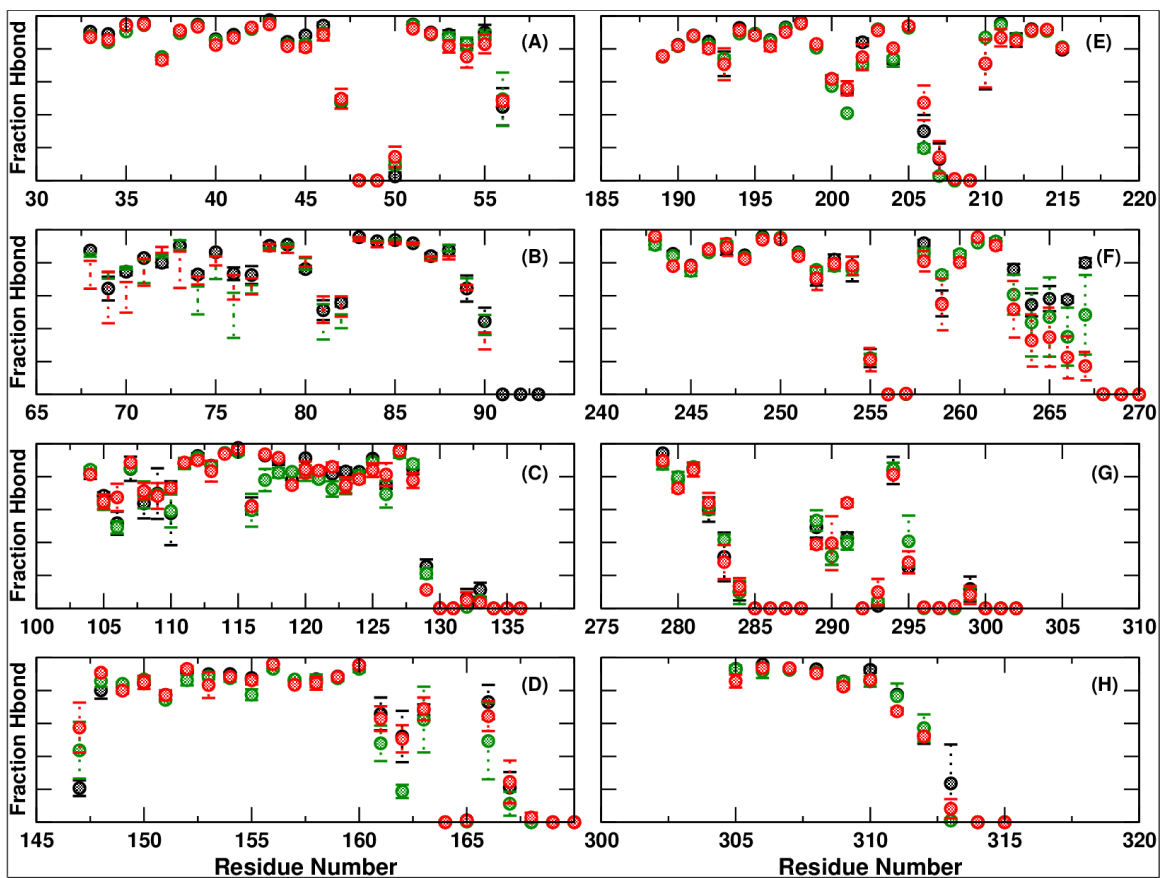


Figure S12: Transmembrane hydrogen bonding between  $i$  and  $i+4$  residues for each of the seven transmembrane  $\alpha$ -helices of CB2, as well as Helix 8 averaged over the last 80 ns of each trajectory. Left Column: (A) helix 1, (B) helix 2, (C) helix 3, (D) helix 4. Right Column: (E) helix 5, (F) helix 6, (G) helix 7, (H) helix 8. 2-12 data is black, 4-12 data is green, and 4-9 data is red.

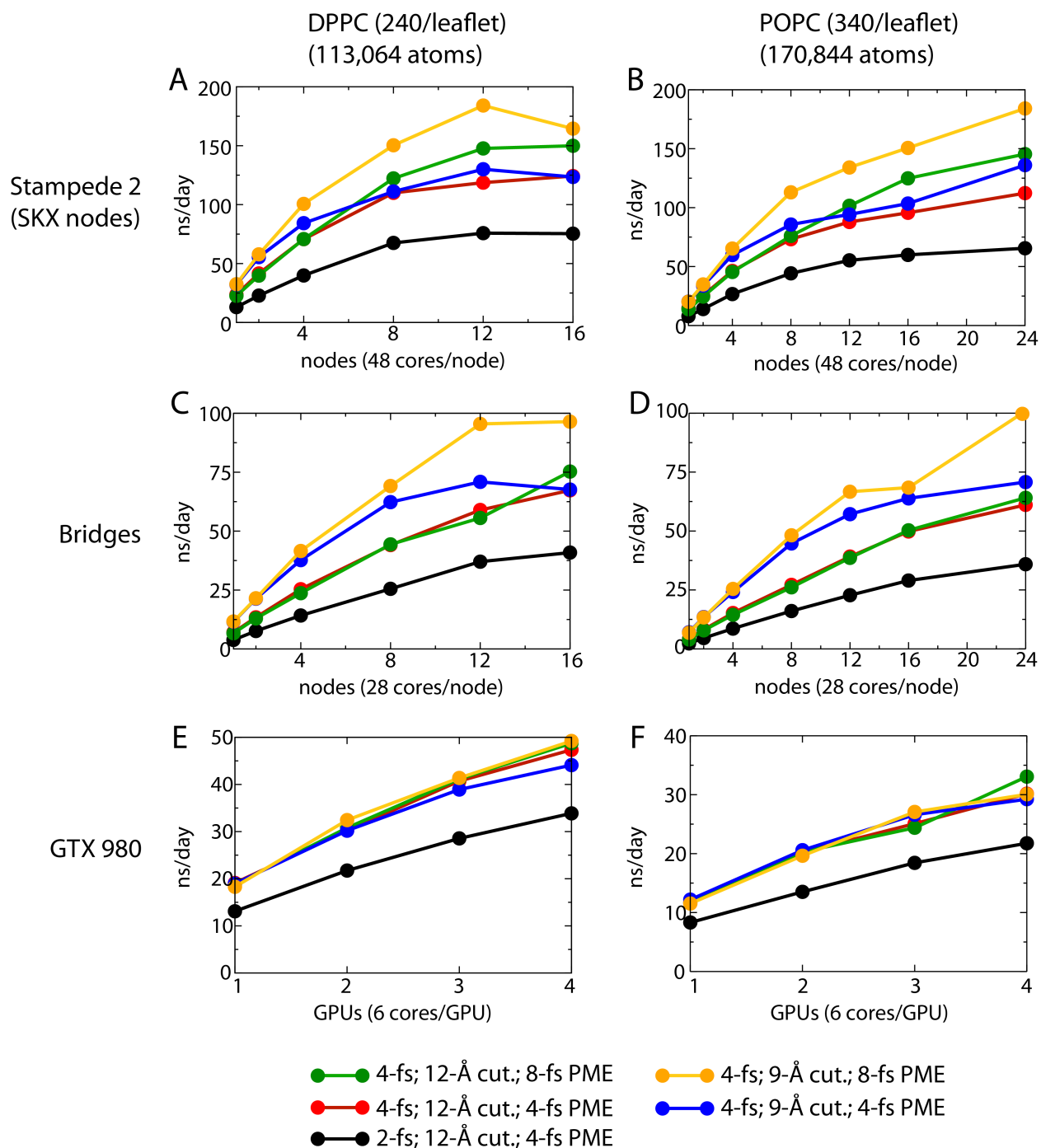


Figure S13: Simulation benchmarks for two membrane systems, DPPC (left column) and POPC (right column) run on (A-B) Stampede 2, (C-D) Bridges, and (E-F) 1-4 GTX 980 GPUs. The GPU version of NAMD used was downloaded on 09/27/18.

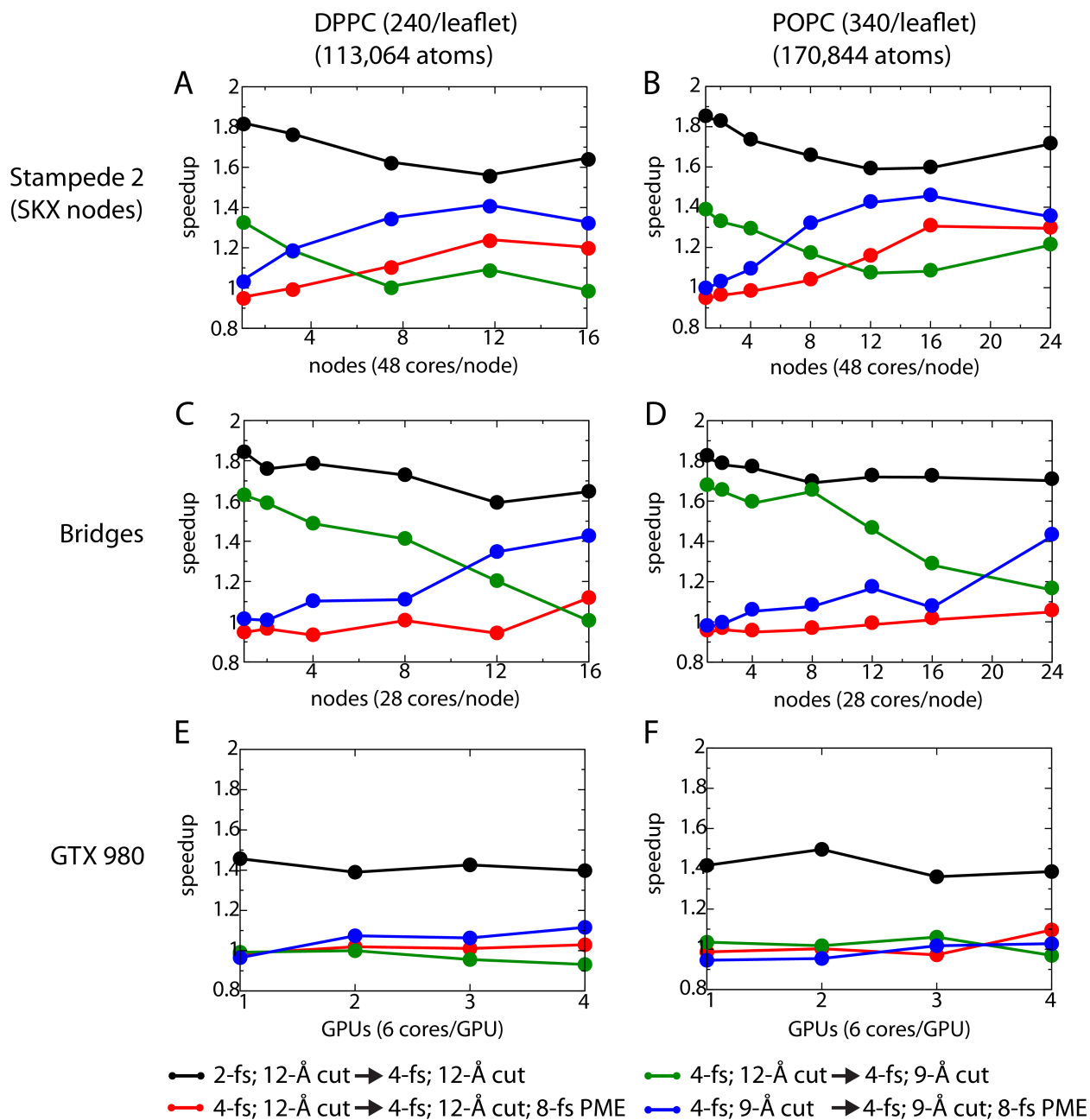


Figure S14: Simulation speedup for two membrane systems, DPPC (left column) and POPC (right column) run on (A-B) Stampede 2, (C-D) Bridges, and (E-F) 1-4 GTX 980 GPUs. For each color, the reference protocol is to the left of the arrow in the legend at the bottom ( $1.0\times$  speedup) and the simulation protocol being compared is to the right of the arrow.

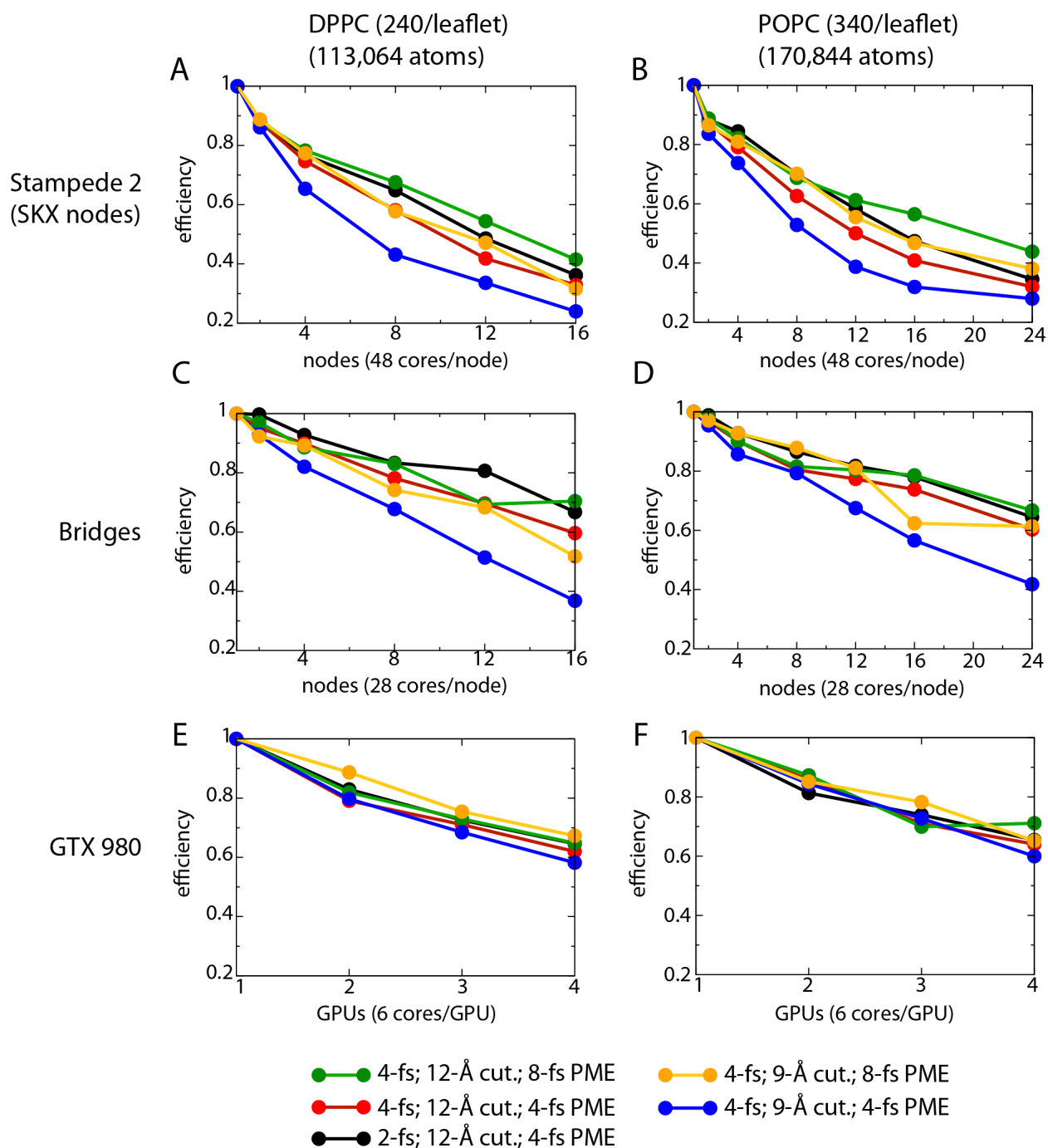


Figure S15: Simulation scaling for two membrane systems, DPPC (left column) and POPC (right column) run on (A-B) Stampede 2, (C-D) Bridges, and (E-F) 1-4 GTX 980 GPUs.